

Influence of corrosive phenomena on bearing capacity of RC and PC beams

Pier Giorgio Malerba^{1a}, Luca Sgambi^{*2}, Diego Ielmini^{1b} and Giordano Gotti^{1c}

¹Department of Civil and Environmental Engineering, Politecnico di Milano, Milano, Italy

²Faculty of Architecture, Architectural Engineering and Urbanism (LOCI), Université catholique de Louvain, Louvain-la-Neuve, Belgium

(Received February 25, 2017, Revised March 3, 2017, Accepted April 13, 2017)

Abstract. The attack of environmental aggressive agents progressively reduces the structural reliability of buildings and infrastructures and, in the worst exposition conditions, may even lead to their collapse in the long period. A change in the material and sectional characteristics of a structural element, due to the environmental damaging effects, changes its mechanical behaviour and varies both the internal stress redistribution and the kinematics through which it reaches its ultimate state. To identify such a behaviour, the evolution of both the damaging process and its mechanical consequences have to be taken into account. This paper presents a computational approach for the analysis of reinforced and prestressed concrete elements under sustained loading conditions and subjected to given damaging scenarios. The effects of the diffusion of aggressive agents, of the onset and development of the corrosion state in the reinforcement and the corresponding mechanical response are studied. As known, the corrosion on the reinforcing bars influences the damaging rate in the cracking pattern evolution; hence, the damage development and the mechanical behaviours are considered as coupled phenomena.

The reliability of such an approach is validated in modelling the diffusion of the aggressive agents and the changes in the mechanical response of simple structural elements whose experimental behaviour is reported in Literature.

A second set of analyses studies the effects of the corrosion of the tendons of a P.C. beam and explores potentially unexpected structural responses caused by corrosion under different aggressive exposition. The role of the different types and of the different positions of the damaging agents is discussed. In particular, it is shown how the collapse mode of the beam may switch from flexural to shear type, in case corrosion is caused by a localized chloride attack in the shear span.

Keywords: corroded R.C. and P.C. beams; time-variant bending and shear capacity; carbonation; chloride attack; corrosion

1. Introduction

*Corresponding author, Assistant Professor, E-mail: luca.sgambi@uclouvain.be

^aFull Professor, E-mail: piergiorgio.malerba@polimi.it

^bStructural Engineer, E-mail: diego.ielmini@virgilio.it

^cStructural Engineer, E-mail: giordano.gotti@hotmail.com

The last decades showed how the R.C. and P.C. structures are susceptible to environmental aggressive agents and how, over time, these phenomena lead to a significant reduction of the load bearing capacity and even to structural collapse.

Large buildings and infrastructures are particularly critical from this point of view, because they are usually exposed to severe environmental conditions (Malerba 2014, Malerba and Sgambi 2014, Sgambi 2014, Köliö *et al.* 2014, Paulík *et al.* 2016).

For this type of structures, it may happen that a local collapse, starting from some damaged detail, leads to sudden and more severe consequences. The collapses of the Berlin Congress Hall (1980) (Isecke 1983), of the Ynys-y-Gwas Bridge in Wales (1985) (Woodward and Williams 1988) and of the Pedestrian Bridge at Lowe's Motor Speedway in North Carolina (2000) (Goins 2000) are known and well-documented examples of failures caused by those degradation phenomena.

The request of an evaluation of the safety level, of the residual bearing capacity and of the expediency and the effectiveness of repairing/refurbishment actions is continuously increasing, for the most important and strategic structures (Biondini *et al.* 2006, Garavaglia *et al.* 2012). Such type of evaluations involves both the analysis of the damaging process evolution and of its mechanical.

This paper presents a computational approach suitable to be used for the analysis of R.C. and P.C. concrete elements subjected to the diffusion of environmental aggressive agents and to the consequent mechanical effects due to corrosion of steel bars and/or tendons.

After a short review of the main physical phenomena that cause the degradation of the concrete structural elements, the first part introduces the analytical models assumed to describe the diffusion of the aggressive agents, the reduction of the steel sections due to corrosion and the mechanical behaviour of R.C. with corroded reinforcement.

In the second part, the criteria to analyse the mechanical behaviour of damaging R.C. and P.C. beams through Finite Element (F.E.) are recalled. Such structural elements are modelled as membranes structures, having non-linear behaviour and susceptible to cracking, according to the hypotheses and the biaxial stress-strain relationships assumed by the Modified Compression Field Theory (M.C.F.T.) (Vecchio and Collins 1986). Special attention has been paid to study the coupling between the damaging acceleration and the cracks widening and propagation. The finite element analysis has been improved, in order to take into account the effects of the corrosion on the reinforcing bars and the dependence of the damaging rate on the cracking pattern evolution, in widening and spacing, under long-term loads.

The third part of the paper is aimed at assessing the reliability of the proposed approach in reproducing the diffusion of the aggressive agents and the changes in the mechanical response of simple structural elements. A set of basic experimental tests reported in Literature and concerning R.C. elements subjected to singular and specific damage actions along time have been selected and comparative numerical analyses have been carried out. The benchmarks regard the modelization of the penetration rate of carbonation and of chlorides into R.C. elements at different levels of cracking and the progression of corrosion and its influence on the ultimate load carrying capacity of slender beams with artificially corroded reinforcement.

The fourth and last part studies the effects of the corrosion of the tendons of an actual P.C. beam and explores potentially unexpected structural responses caused by corrosion. As known, the overall static behaviour and load bearing capacity of R.C. structural element depends on its material characteristics (concrete and steel), on its sectional properties, on the reinforcement layout and on the loading distribution. A change in one or more of these characteristics, due for instance to some damaging cause, determines a change in the element behaviour too. The method is applied

in modelling the load path for P.C. beams under a different aggressive exposition. The role of the different types and of the different positions of the damaging causes is discussed. A result, which is worth outlining, concerns the case of a localised chloride attack in the shear span of P.C. beams. For such a case, it is shown how the corrosion could switch the collapse mode from a flexural collapse to a shear one.

The paper concludes in outlining the modelling capabilities of the proposed approach and in presenting its wide range of application.

2. Characterisation of the damaging environment

2.1 General aspects

Degradation affects both concrete and steel and it is highly dependent on the processes by which the water and the potential aggressive agents (carbon dioxide, chlorides, sulphates, etc.) migrate from the external environment into the concrete mass (Coronelli *et al.* 2009, Lu *et al.* 2016, Michel *et al.* 2016).

These processes are not instantaneous; they occur gradually over a period of time and are influenced by the characteristics of the ambience and of the materials.

With respect to the ambience, we can distinguish between physical factors (the seasonal ranges of temperature and of humidity conditions), and the chemical ones (Ekolu 2016). Among these, in particular, the CO₂ percentage present in the air and the chloride and sulphates concentration in exposed surfaces are considered.

As regards to the materials, the durability of the concrete is strongly influenced by the water-cement ratio and by the cement content. The steels durability depends on their type and grade, being known that the stress corrosion phenomenon makes the prestressing steels more vulnerable to corrosion with respect to the ordinary ones (Tuutti 1982, Nürnberger 2002, Bertolini *et al.* 2004). Special additives may improve the basic characteristics of the concrete. In some applications, special surface protections, like resins and zinc coatings, may improve the steels performance over time.

Other damaging phenomena are of mixed type (physical/chemical/mechanical), as in the case of the relative influence among alkali-silica reactions, freezing and thawing cycles, repeated loading effects and crack propagation. Such kind of processes widens the preferential paths through which the aggressive agents diffuse in the concrete mass and accelerates corrosion and damage of the structural element (Vesikari 1988, Breyse 1997, Vořechovská 2009).

In the development of these damaging processes, two different phases must be identified and clearly distinguished: the incubation time, during which the external aggressive agents penetrate into the concrete cover and cause a progressive destruction of the protective film formed around the bars in an alkaline environment, and the onset and the propagation of corrosion (Tuutti 1982).

2.2 Definition of damaging environment

In the following, the typical microclimate conditions, which surround the bridges girders, will be considered. The external surfaces of the structural elements of a girder are exposed to the carbon dioxide present in the atmosphere, which, interacting with the calcium hydroxide of the concrete, triggers the carbonation. The exposure conditions may be different, but the carbonation

process must be considered always active on any sort of concrete surface exposed to the air.

Another source of damaging is the chloride penetration. Since the middle of last century, de-icing salts have been used in order to make the runability of the main roadways safer during the cold season. The washing and the percolation of salted water feed the penetration of chlorides into the concrete mass, frequently fostered by the action of freezing and thawing cycles. The chloride penetration may surround the whole exposed surfaces or may be localised around some particular sections, as, for instance, those in proximity of the ducts of the drainage system.

Both phenomena are influenced by the actual state of the concrete surface. A high concrete porosity, a low quality of the road construction as well as unfavourable curing conditions accompanied by a wide initial microcracking enhance the propagation phenomena and accelerate the onset of corrosion.

The evolution of these aggressive agents within the concrete volume can be analysed through analytical equations and suitable computational models, corroborated by wide comparisons with the results of experimental tests and of a posteriori controls on bridges in service.

A specific study was focused on coupling between the damaging acceleration and the cracks widening and propagation. Being mainly interested in the analysis of the mechanical effects of corrosion, the propagation of the damage causes over time is modelled through analytical equations suitable to deal both with sound and cracked concrete.

2.3 Definition of damaging environment

2.3.1 Carbonation model

The hydration of cement paste gives origin an alkaline environment, having approximately $\text{pH}=12\div 13$, which protects steel from corrosion. However, this protection is destined to vanish over time as the carbon dioxide in the atmosphere reacts with calcium hydroxide, producing calcium carbonate and water. This reaction results in a lowering of pH. When pH drops below $10\div 11$, the steel is no longer protected against oxidation. This pH limit is defined as the point of steel depassivation.

The carbonation reaction begins on the external surfaces and, over time, penetrates into the concrete element. We are interested in evaluating the penetration depth of the carbonation over time and in computing the time required by the chemical reaction to carbonate the entire concrete cover. We distinguish between penetration in sound and in cracked concrete.

Uncracked concrete. Many models of carbonation penetration exist. For uncracked concrete, they can all be synthetically resumed in following equation

$$x(t) = K \cdot t^{1/n} \quad (1)$$

where $x(t)$ is the thickness of the carbonated layer (mm), K is the carbonation coefficient ($\text{mm}/\text{year}^{1/2}$) and t is the time (years). For the more common types of concrete, the index n has an approximate value of 2.0, so carbonation depth grows with a parabolic progression

$$x(t) = K \cdot \sqrt{t} \quad (2)$$

In low-porosity compact concrete, n is greater than 2.0 and the penetration velocity decreases (Bertolini 2004). The coefficient K depends on environmental factors (humidity, temperature and contents of CO_2 in the air) and on concrete characteristics (type and contents of cement, water/cement ratio, curing conditions, porosity). Usually, following values are assumed: $2 < K < 5$

for compact concretes, with a cement contents greater than 3.50 kN/m^3 ; $5 < K < 8$ for medium compactness concretes; $K > 8$ for poor concretes, with cement contents below 2.50 kN/m^3 .

Cracked concrete. When the tensile stress exceeds the corresponding strength, concrete cracks. The total tensile stress may be the result of different contributions: mechanical, due to the acting loads; distortional, due to creep and shrinkage; environmental, due to temperature exposition or to freezing-thawing cycles.

Carbonation penetration is higher through cracks. According to Vesikari (1988), the carbonation depth is computed through the following equation, which also takes into account the crack width

$$x(t) = 50 \cdot \sqrt{w} \cdot \sqrt[4]{t} \quad (3)$$

In this relationship $x(t)$ is the thickness of the carbonised layer (mm), w is the width of the crack (mm) and t is the time (years). If no aggressive agents are present, the cracking reduces the stiffness of a structural element, but it does not influence its ultimate bearing capacity. In the service ambience, cracks foster the penetration of carbon dioxide and reduce the corrosion initiation time of steel. Hence, a sound evaluation of carbonation depth and carbonation velocity has to take into account the mechanical response of the structure.

2.3.2 Chloride diffusion model

The time required to reach a critical chloride concentration C_{cr} on the reinforcement surface depends on the chloride concentration on the concrete external surfaces, on the cement matrix characteristics, on the thickness of the concrete cover, and on the cracking state. The critical value C_{cr} ranges from 0.4% to 1% in mass with respect to the cement contents. An average value for well compacted concretes is 0.6%.

Uncracked concrete. Considering uncracked concrete as a porous material and chloride propagation as a diffusion process, a close approximation of chloride concentration profiles over time is predicted by Fick's second law, according to the differential equation that follows

$$\frac{\partial C(x,t)}{\partial t} = \frac{\partial}{\partial x} \left[D(x,t) \cdot \frac{\partial C(x,t)}{\partial x} \right] \quad (4)$$

where x is the penetration depth, measured from the reference external surface (mm), t is the time (years), $C(x,t)$ is the chloride concentration (mass % with respect to the cement contents) and $D(x,t)$ is the diffusion coefficient (mm^2/sec).

An analytical solution of Eq. (4), can be obtained if we assume that the chloride content on the external surface C_s remains constant over time and that the diffusion coefficient $D(x,t) = D_{app}$ remains constant over time and in the space. Under these hypotheses, the concentration of chlorides at the depth x and at the time t is given by following equation

$$C(x,t) = C_s \left[1 - \operatorname{erf} \left(\frac{x}{2 \cdot \sqrt{D_{app} \cdot t}} \right) \right] \quad (5)$$

where erf is the Gauss error function and $D_{app} = 10^{-7} \div 10^{-5}$ (mm^2/s) is the so called apparent (effective) diffusion coefficient. This equation can be used to determine when the critical chloride concentration is reached and steel corrosion starts.

Cracked concrete. In the design practice, the diffusion coefficient may be assumed as constant, even if it actually depends on many chemical, physical and mechanical phenomena, which vary

over time and influence the chloride penetration process.

Many studies have been performed regarding the parameters that affect the initiation of steel corrosion in cracked concrete (Malumbela 2009, El Hassan *et al.* 2010). As noted before, the cracks constitute preferential pathways for chloride penetration, thus reducing the time required for the onset of corrosion (Otsuki *et al.* 2000). When the width of the cracks is relatively small, even if corrosion has been triggered, the corrosion products can seal the cracks, at least in the areas closer to the reinforcement, and even re-establish some protective film on the reinforcement bars (Jacobsen *et al.* 1996, Schiessl and Lay 2005).

In truth, studies performed at the L.M.D.C. Lab (Toulouse) have shown that the influence of cracks on the corrosion process is not significant as long as the crack width is below 0.3 mm (Vidal *et al.* 2007). On the contrary, wider cracks markedly modify the diffusion process.

Dealing with R.C. and P.C. cracked elements, Fick's second law can still be used if, according to Boulfiza *et al.* (Boulfiza *et al.* 2003), the apparent diffusion coefficient D_{app} is replaced by an average diffusion coefficient D_{av}

$$D_{av} = D_{app} + \frac{w}{s_{m\theta}} \cdot D_{crk} \quad (6)$$

where w is the crack width, $s_{m\theta}$ is the crack spacing and $D_{crk} \cong 5 \cdot 10^{-4} \text{ mm}^2/\text{s}$ is a new diffusion coefficient (Boulfiza *et al.* 2003) to be adopted in the cracked zones. Substituting the average D_{av} to D_{app} in Eq. (5), one obtains

$$C(x, t) = C_s \cdot \left[1 - \text{erf} \left(\frac{x}{2 \cdot d} \right) \right] \quad \text{where } d = \sqrt{D_{av} \cdot t} \quad (7)$$

In the following, the apparent diffusion coefficient D_{app} is used, in accordance with Eq. (5), either in uncracked zones of the structure or where the crack opening is below 0.3 mm. In the cracked zones having $w \geq 0.3$ mm, the average diffusion coefficient D_{av} and Eq. (7) is used.

2.4 Steel corrosion model

When the carbonation front and/or the critical chloride concentration reaches the surface of the reinforcing steel and when suitable quantities of water and oxygen are present, the corrosion process starts. The main consequences of steel corrosion are:

- A reduction of the sectional area of the bars and, hence, of the bearing capacity of the reinforcement.
- The onset of further damages in the concrete volume due to the expansive oxides produced by the corrosion. As known, the oxides produced by the corrosion are subjected to a volumetric expansion from 1 to 4÷5 times that of the ferrous material from which they are generated. Such an expansion produces further cracking, reduces the bonding of the reinforcement in the concrete and causes spalling at the corners of the section and delamination of the concrete cover (Bertolini *et al.* 2004).

The corrosion processes in normal and prestressing steels are quite different. In normal steel, the corrosion involves the whole circumference of the bar. In prestressing steel, the corrosion is usually localised (pitting).

2.4.1 Corrosion model for standard reinforcement

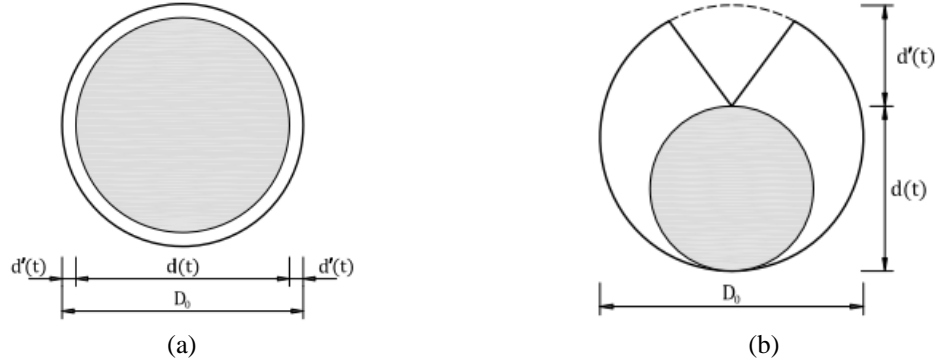


Fig. 1 Geometry of the corroded reinforcing bar, (a) uniform corrosive attack and (b) corrosive attack on one side only

By reinforcement degradation we mean a reduction of the cross-sectional area of the bars without changes of their Young's modulus. Moreover, the corrosion phenomenon depends on the aforementioned environmental conditions, on the material characteristics and on the integrity of the concrete volume.

Several models are presented in the RILEM Report 14 (Sarja and Vesikari 1996). The most widely used gives the effective area of reinforcement $A_s(t)$ (mm^2), reduced by corrosion, as follows

$$A_s = \begin{cases} \frac{N_s \cdot \pi \cdot D_0^2}{4} & \text{if } t \leq t_0 \\ \frac{N_s \cdot \pi \cdot [D_0 - n \cdot d'(t)]^2}{4} & \text{if } t > t_0 \end{cases} \quad (8)$$

where N_s is the number of reinforcing bars, D_0 is their initial diameter (mm), $d'(t)$ is the depth of corrosion (Fig. 1) (mm), t_0 is the time of corrosion initiation (years), $n=(1, 2)$ is a coefficient that takes into accounts the possibility of the attack coming from one or two sides of the reinforcing bar.

At the time t , the depth of the corrosion of the corroded reinforcing bar $d'(t)$, which appears in Eq. (8), is estimated through Faraday's law

$$d'(t) = 0.0116 \cdot i_{corr} \cdot (t - t_0) \quad (9)$$

where i_{corr} is the corrosion current per unit area ($\mu\text{A}/\text{cm}^2$), t is the total time (years) since the completion of the building and 0.0116 is a conversion factor from $\mu\text{A}/\text{cm}^2$ to $\mu\text{m}/\text{year}$. According to this formulation of Faraday's law and in the case of steel, a corrosion current of $1 \mu\text{A}/\text{cm}^2$ corresponds to a diameter decrease of $11.60 \mu\text{m}/\text{year}$.

Then, reinforcing bar diameter $d(t)$, as function of time, can be estimated as

$$d(t) = D_0 - n \cdot d'(t) \quad (10)$$

and results linear over time.

2.4.2 Corrosion model for prestressing reinforcement

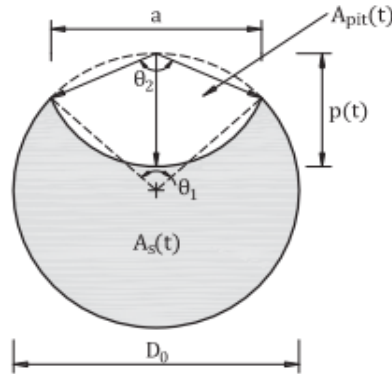


Fig. 2 Geometry of localised corrosion of prestressed steel

Prestressing steel is prone to many forms of corrosion, such as stress corrosion, hydrogen embrittlement, corrosion fatigue, and fretting corrosion (Nürnberg 2002).

The corrosion triggered by chloride attacks produces localised cavities (pits) and its action is usually called pitting.

Being the diameters of the wires (5÷7 mm) relatively small in comparison to the diameters of the reinforcing bars, a decrease of the sectional area of the wires produces disproportional loss of the bearing capacity and, over time, it may cause sudden failures with catastrophic consequences.

The maximum depth of corrosion (p_{\max}) due to pitting in a wire or in a bar is usually greater than the average depth measured for generalised corrosion $p_{av}=d'(t)$. The ratio

$$R = \frac{p_{\max}}{p_{av}} = \frac{p_{\max}}{d'(t)} > 1 \quad (11)$$

is called pitting factor. Various methods and criteria have been used to assign a numerical value to the pitting factor: for Gonzalez *et al.* (Gonzalez *et al.* 1995) the value of R ranges from 4 to 8; for Darmawan and Stewart (2007), $R=8\div 11$; for Tuutti (1982), $R=4\div 10$.

In addition, the cavity generated by the pitting attack may have different geometries. For the sake of simplicity, Val *et al.* (1998) model this cavity through a hemispherical surface, as shown in Fig. 2. For a depth of the pit at time t equal to $p(t)=d'(t) \cdot R$, the sectional area of a wire or of a bar is

$$A_s(t) = A_0 - A_{pit}(t) = \frac{\pi \cdot D_0^2}{4} - A_{pit}(t) \quad (12)$$

where A_0 is the initial area and $A_{pit}(t)$ results from geometry, as shown in Fig. 2 and detailed in the Appendix 1.

3. Mechanical behaviour. Recall of the modified compression field theory

The mechanical behaviour of R.C. and P.C. elements is now considered.

3.1 Concrete biaxial stress-strain relationships

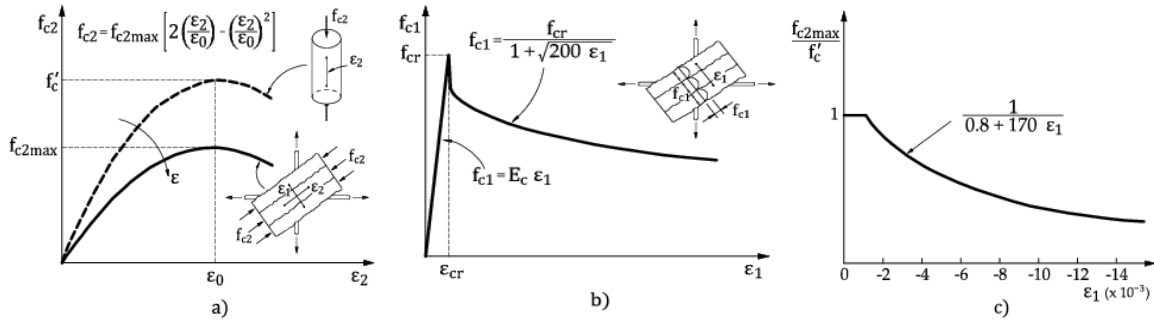


Fig. 3(a) Stress-strain relationship for cracked concrete in compression ($\varepsilon_0=0.002$), (b) maximum compressive stress as function of the principal tensile strain, (c) average stress-strain relationship for cracked concrete in tension ($E_c=2 \cdot f_{c2max}/\varepsilon_0$)

By means of the F.E.M., R.C. and P.C. beams are modelled as membranes structures, having non-linear behaviour and being susceptible of cracking. The general hypotheses and the biaxial stress-strain relationships according to the Modified Compression Field Theory (MCFT) are assumed (Vecchio and Collins 1986, Vecchio 1989, Bontempi *et al.* 1996, Sgambi 2004, Sgambi *et al.* 2006, Zhang *et al.* 2012, Palermo *et al.* 2014, Sgambi *et al.* 2014).

The MCFT considers a constant thickness membrane element, made of a matrix of concrete and reinforced by two orthogonal orders of bars. No overall slip between reinforcement and concrete is considered. The element has finite size, but it is treated as an infinitesimal: within the element, the stress field is constant and, during deformations, the boundary edges move and rotate remaining straight. For a given membrane state of stress or strain, the relationships between the stresses acting on the edges and the corresponding strains comply with following hypothesis:

1. The R.C. is a non-linear composite elastic material.
2. Equilibrium and compatibility are formulated in terms of average stresses and average strains, referred to areas which are sufficiently wide to contain a defined crack pattern.
3. In a general biaxial state, the direction of the principal compression strain ε_1 and that of the principal compression stress f_{c1} are correlated in a narrow band ($\theta_c \approx \pm 10^\circ$). Therefore, we assume that the principal strain axes and the principal stress axes coincide.
4. Prior to the cracking strain ε_{cr} , the principal tensile stress f_{c1} is linear with ε_1 and with an initial tangent modulus E_c . After ε_{cr} , in order to take the tension stiffening effects into account, f_{c1} decreases with the increasing values of ε_1 , as shown in Figs. 3(a) and 3(b).
5. The principal compressive stress f_{c2} , corresponding to the principal strain ε_2 , depends on the strain softening effect, due to the principal tensile strain ε_1 . The strength $f_{c2,max}$ diminishes with ε_1 and the stress-strain relationship changes in affinity with $f_{c2,max}$, as shown in Fig. 3(c).
6. For the reinforcement, bilinear elastoplastic stress-strain relationships are assumed.
7. The possibility of transmitting the average tensile stress f_{c1} across the cracks has to be verified.

3.2 Tension stiffening in the membrane states

In a cracked R.C. element (Fig. 4(a)), the tensile stress at a crack is zero in the concrete, and it is maximum in the reinforcement ($f_{sx}=f_{sx,cr}$; $f_{sy}=f_{sy,cr}$). Between the cracks, the tensile stresses are

transferred from the steel to the concrete by the bond action that develops along the bars. In this way, concrete contributes in carrying the tensile forces and in increasing the overall stiffness of the structure (tension stiffening).

Moreover, a sliding resistance occurs between the crack interfaces, due to the aggregate interlock. This action may be accounted for by a relationship between a containment stress f_{ci} , normal to the crack, and a corresponding shear stress $v_{ci} = v_{ci}(f_{ci})$ (Fig. 4(c)). On the other hand, adopting constitutive laws dealing with average values, the stresses on sections parallel to the cracks are those shown in Fig. 4(b). Between these two sets of stress, following conditions of static equivalence are required

$$\rho_{sx} \cdot f_{sx} \cdot \sin \vartheta + f_{c1} \cdot \sin \vartheta = \rho_{sx} \cdot f_{sx,cr} \cdot \sin \vartheta - f_{ci} \cdot \sin \vartheta - v_{ci} \cdot \cos \vartheta \quad (13)$$

$$\rho_{sy} \cdot f_{sy} \cdot \cos \vartheta + f_{c1} \cdot \cos \vartheta = \rho_{sy} \cdot f_{sy,cr} \cdot \cos \vartheta - f_{ci} \cdot \cos \vartheta - v_{ci} \cdot \sin \vartheta \quad (14)$$

These equations limit the average tensile stress $f_{c1} = f_{c1}(\varepsilon_1)$. The limits arise from the yielding of the steel reinforcement ($f_{sx} = f_{yx}$; $f_{sy} = f_{yy}$) and/or from the limited shear transfer capacities deriving from the aggregate interlock.

3.3 Check of equilibrium in the cracked state

The average tensile stress in the concrete f_{c1} , corresponding to a given principal strain ε_1 , satisfy the equilibrium and the yielding conditions, if a combination of the shear and of the compressive stresses v_{ci} and f_{ci} is found, compatible with an assumed interface shear transfer law. Otherwise, f_{c1} has to be reduced until a solution is possible (Vecchio and Collins 1986). More simply, if one assumes that, independently of the value of f_{ci} , a balancing shear stress v_{ci} may develop, then f_{c1} can be transmitted across the cracks, if following upper limit is respected (Vecchio 1989)

$$f_{c1} \leq \rho_{sx} \cdot (f_{yx} - f_{sx}) \cdot \sin^2 \theta + \rho_{sy} \cdot (f_{yy} - f_{sy}) \cdot \cos^2 \theta \quad (15)$$

4. Coupling damage evolution and mechanical behaviour

The Finite Element analysis based on the Modified Compression Field Theory has been modified in order to take into account the effect of corrosion on the reinforcing bars and the dependence of the damaging rate on the cracking pattern evolution, in widening and spacing, under long-term loads.

4.1 Incremental formulation of the carbon dioxide and chloride propagation

The onset of cracks and their propagation widen the preferential paths through which the aggressive agents diffuse in the concrete mass and accelerate the corrosion of steel elements. As stated before, damage evolution and mechanical behavior are coupled phenomena. This means that, in dealing with the carbon dioxide and chloride propagation, the parameters that condition the penetration of these aggressive agents change. Therefore, they should be updated according to the new damaged state of the media.

Expanding in Taylor's series the equations that compute the carbonation depth and the chloride concentration over time, with respect to the time t , we obtain following result from Eq. (3)

$$x(t + \Delta t) = x(t) + \frac{dx(t)}{dt} \cdot \Delta t + o(t^2) = x(t) + \left(\frac{25 \cdot w'(t) \cdot \sqrt[4]{t}}{\sqrt{w(t)}} + \frac{25}{2} \cdot \frac{\sqrt{w(t)}}{\sqrt[4]{t^3}} \right) \cdot \Delta t + o(t^2) \quad (16)$$

and, from Eq. (7)

$$\begin{aligned} C(x, t + \Delta t) &= C(x, t) + \frac{dC(x, t)}{dt} \cdot \Delta t + o(t^2) = \\ &= C(x, t) + C_0 \cdot \frac{2}{\sqrt{\pi}} \cdot \frac{[D_{cr} \cdot w'(t) \cdot t + D_{cr} \cdot w(t) + D_{app} \cdot S_{m\theta}] \cdot x}{4 \cdot t \cdot [D_{cr} \cdot w(t) + D_{app} \cdot S_{m\theta}] \cdot \sqrt{\left(D_{app} + \frac{w(t)}{S_{m\theta}} \cdot D_{cr} \right) \cdot t}} \cdot E_{ws} \end{aligned} \quad (17a)$$

where

$$E_{ws} = \exp \left[- \left(\frac{x}{2 \cdot \sqrt{\left(D_{app} + \frac{w(t)}{S_{m\theta}} \cdot D_{cr} \right) \cdot t}} \right)^2 \right] \cdot \Delta t + o(t^2) \quad (17b)$$

The rate of cracking w' is difficult to determine. Moreover, sensitivity analyses showed that its influence on the updated values of $x(t + \Delta t)$ and on $C(x, t + \Delta t)$ is little. Hence, it has been neglected in these computational model.

4.2 Criteria for sampling the structural behavior over time

From the mechanical point of view, the measure of damage is given by the reduction of the bearing area of reinforcing and prestressing steel. During the analysis, these areas are updated over time according to the evolution of the influence of the aggressive agents causing corrosion.

The sequence of the analysis is organized as follows:

- Environmental and material data, necessary to define the constant K in Eq. (2) and the constants C_s , D_{app} and D_{crk} in Eq. (7), are given.
- The structure is completely defined in geometry, mechanical materials characteristics and prestressing intensity.
- A sustained constant load is assumed. The load intensity is a percentage of the ultimate one, close to the permanent load in a bridge structure (for example 60%).
- The analysis starts and is repeated over time, according to assumed time intervals. For each step of analysis, displacements, cracking patterns, compressive and tensile stress are stored and filtered for significant control sections.

Further details will be given for the cases studied in the following.

5. Validation of the model

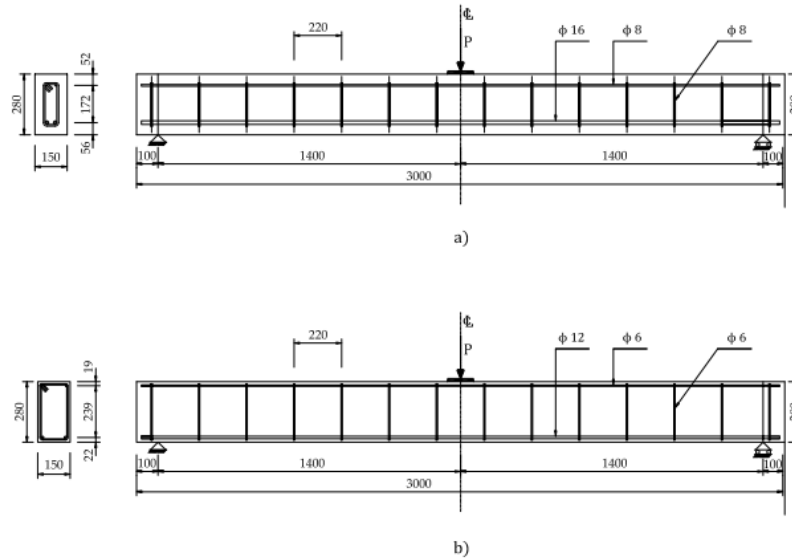


Fig. 5 LMDC beams. Type A (a) and type B (b) beam geometries

Table 1 Material properties (the values in brackets are not explicitly reported in the references, but assumed for computations)

Concrete	f'_c (MPa)	f_{cr} (MPa)	ε'_c (%)	E_c (MPa)	
	-45	4.7	(-0.002)	32000	
Steel (top layer)	f_y (MPa)	f_u (MPa)	ε_{su} (%)	E_s (MPa)	A_s (mm ²)
	500	(700)	16	(196000)	56.55
Steel (bottom layer)	f_y (MPa)	f_u (MPa)	ε_{su} (%)	E_s (MPa)	A_s (mm ²)
	500	(700)	(16)	(196000)	226.19

Table 2 Dimensions, cover thickness and load levels for beams A1, A2 and B1, B2

l×h×b	Beam Type A		Beam Type B	
		3000×280×150	3000×280×150	(mm)
Cover	c_i	$c_A=40$	$c_B=10$	(mm)
Load Level 1	1	13.5	13.5	(kNm)
Load Level 2	2	21.2	21.2	(kNm)

With reference to specific experimental tests reported in Literature, the present approach is validated in modelling the diffusion of the aggressive agents and the changes in the mechanical response of simple structural elements. Each test concerns a single and specific damage action acting over time. With reference to slender R.C. beams, tested after artificial corrosion processes, the benchmarks regard the capacity of this F.E. modelling approach (a) the rate of carbonation penetration and of chlorides into R.C. elements at different levels of cracking, (b) the progression of corrosion, (c) the influence of corrosion on the loading path, on the crack propagation and on the ultimate load carrying capacity.

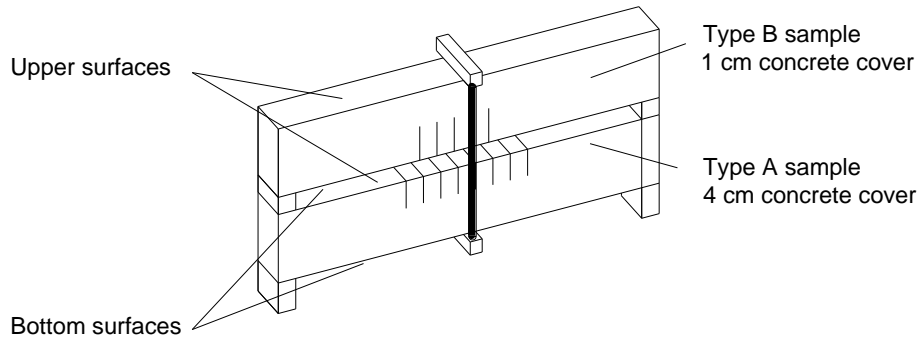


Fig. 6 LMDC beams (Castel *et al.* 1999). Loading system in three-points flexion

5.1 Modellization of the carbonation and chloride penetration

In the '80/'90 of the past century, a wide experimental program on the effects of the aggressive environmental agents on the mechanical behaviour of R.C. beams had been carried out (Castel *et al.* 1999, Castel *et al.* 2000, Vidal *et al.* 2007) at the Laboratoire Matériaux et Durabilité des Constructions (LMDC), Toulouse (France). Within the LMDC tests, we consider a set of rectangular beams having the same overall dimensions, but different cover thickness (Fig. 5), and subjected to constant concentrated loads, sustained for 13 years under different exposure conditions. Tables 1 and 2 summarize, respectively, the characteristics of the materials and the beam dimensions.

The beams were tested in couples (A1 with B1, A2 with B2), according to the setup shown in Fig. 6. One couple of specimens was exposed to natural weather conditions, but protected from rain, in order to study the development of carbonation. Another couple was maintained in a confined environment containing chloride, in order to study the influence of this specific chemical agent on the corrosion of the reinforcement.

In the following, the experimental results will be compared with the numerical ones, developed according to the model proposed in the previous paragraphs.

5.1.1 Penetration of carbonation in a progressive cracking pattern

We consider the couple of beams A2 and B2, exposed to natural weather conditions and subjected to the same load for the same time (13 years). Under these conditions, we expect that the different cover thicknesses ($c_A=40$ mm, $c_B=10$ mm), the different response to cracking and the different distribution of cracking along the span cause perceptible differences in the penetration of the carbonation. The depth of carbonation was experimentally measured every 20 cm along the intrados of beam B and along the extrados of beam A, in the fields between the couples of stirrups, in order to avoid local interferences from the steel bars.

The F.E. models of the beams are shown in Figs. 7(a), (b). Based on the characteristics of the cement paste and of the concrete mix, a coefficient of carbonation $K=3.3$ mm/year^{1/2} and a corrosion rate $i_{cor}=0.055$ mm/year have been assumed in the analysis.

The results are shown in Figs. 7(a) and 7(b). Each figure shows: (i) the comparison between carbonation depths measured along the beam and obtained respectively from the experimental measurements and the F.E. analysis; (ii) the comparison between the corresponding crack patterns. In both beams the F.E. model is suitable to foresee how the depth of carbonation increases from

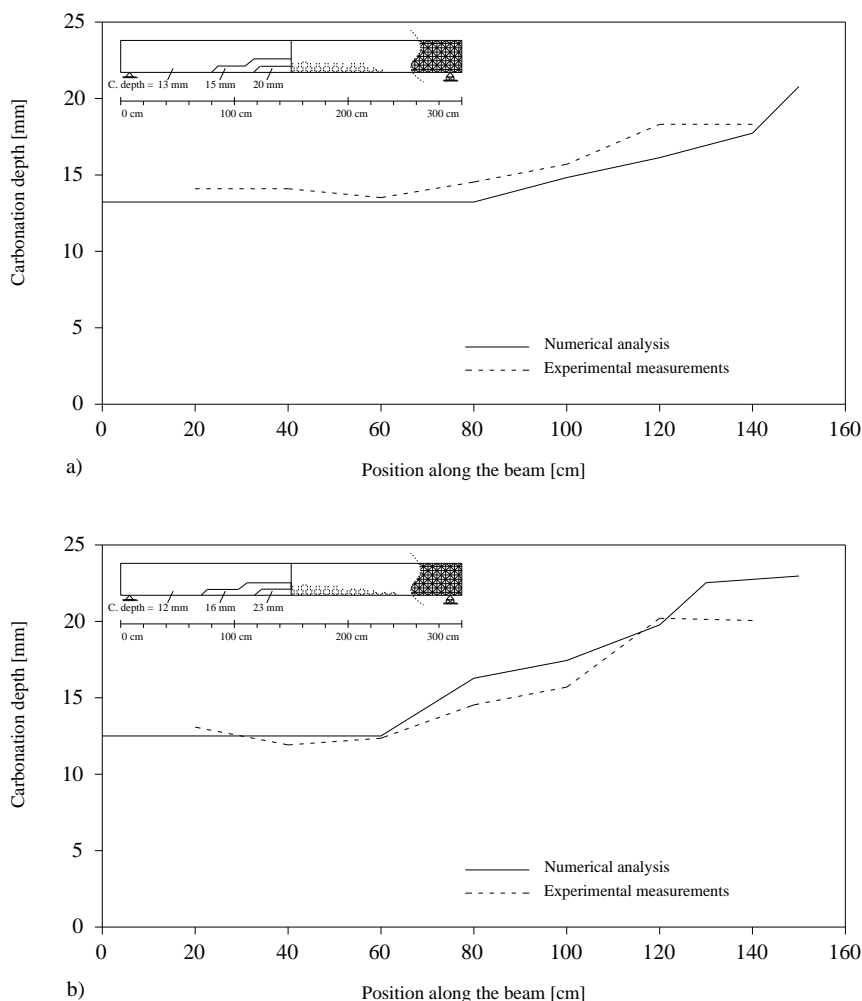


Fig. 7 LMDC beams. Numerical and experimental carbonation depth and cracking extension after 13 years for A-type beam (a) and B-type beam (b)

the support to the middle and how such an increase is higher for beam B (+58%) with respect to beam A (+35%). The numerical results show slightly higher crack widths and wider crack propagation in beam B, which has a thinner cover depth than beam A.

5.1.2 Penetration of chloride in a progressive cracking pattern

Other LMDC tests were carried out on couples of beams type A and B in a climate room; the beams were loaded as before and surrounded by a saline fog (Fig. 8). The salt concentration was 35 g/l of NaCl, nearly equal to that of sea water. The experiment lasted 17 years. In the first six years, the beams were continuously sprayed. From the sixth to the ninth year, they were sprayed every second week, alternating weeks of wet and dry conditions. During those years, the beams were kept indoor at a temperature of 20°C. After the ninth year, the climate room was placed outdoors and exposed to temperatures ranging from -5°C to 35°C. The weekly alternating spraying continued until the seventeenth year (Vidal *et al.* 2007).

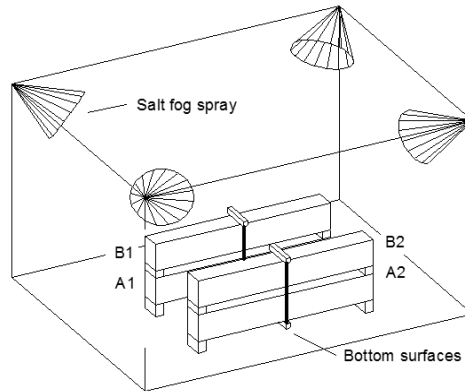


Fig. 8 LMDC beams (Castel *et al.* 2000). Experimental room and loading system in three-points flexion

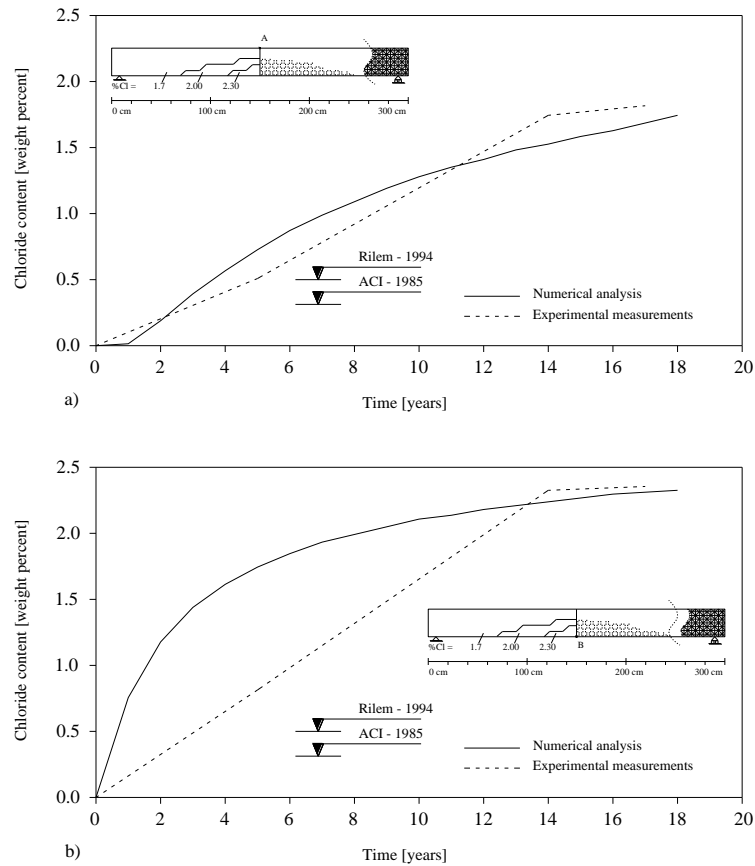


Fig. 9 Variation per years of chloride content at the depth of the reinforcement (16 mm) in the compression zone (a) and in the tension zone (b) of the corroded beam. Comparison between the numerical analysis and the experimental results obtained by Castel *et al.* (2000)

The chloride content was measured at midspan and at the depth of the compressed and tensioned fibres, i.e., at the level of the reinforcement bars.

Table 3 Main characteristics of the beams tested by Almusallam *et al.* (2001)

Length	Height	Width	Span	Cover	Reinforcement
l_0 (mm)	h (mm)	b (mm)	l (mm)	c (mm)	A_s (mm ²)
812	63.5	305	711	9.5	$5 \times 0.2827/57$

Table 4 Mechanical properties of the beam tested by Almusallam *et al.* (2001) (the values in brackets are not explicitly reported in the references, but assumed for computations)

Concrete	f_c' (MPa)	f_{cr} (MPa)	ε_c' (%)	E_c (MPa)	
	-30	(1.81)	(-0.002)	(30000)	
Steel	f_y (MPa)	f_u (MPa)	ε_{su} (%)	E_s (MPa)	A_s (mm ²)
	475	(750)	(14)	(200000)	141

The F.E. models of the beams are shown in Figs. 9(a), (b). In the analysis, following parameters were assumed: (a) surface chloride content $C_s=0.35\%$, (b) effective diffusion coefficient of chloride of $D_{ce}=5 \times 10^{-13}$ m²/sec, (c) diffusion coefficient in the cracked zone of $D_{ce}=1 \times 10^{-9}$ m²/sec, (d) corrosion rate $i_{corr}=0.122$ mm/year. The results are shown in Figs. 9(a) and 9(b).

The figures show: (i) the comparison between the total content of chlorides (CC, weight percentage, with respect to the cement content), measured at the depth of the reinforcement (16 mm) in the compression zone (a) and in the tension zone (b); (ii) (b) the comparison between the corresponding crack patterns.

In the compression zone, the agreement between numerical and experimental chloride contents along time is good. For the tension zone, the agreement is good towards the end of the experiment, while the intermediate measurement at the fifth year differs sensibly. This gap can be mainly ascribed to the measurement technique used in the early years of the experimental test, which was less precise than the one used at the end, as reported in (Vidal *et al.* 2007). After 3÷4 years, it can be observed that CC exceeds the level assumed as critical by ACI-1985 (0.3%) and by RILEM-1994 (0.5%). Between the fourteenth and the seventeenth year, CC tends to stabilize, by reaching the saturation limit (maximum chloride content in the concrete). The comparison between the corresponding crack patterns results fairly good as it concerns both depth and horizontal distribution.

5.2 Corrosion propagation and ultimate bearing capacity

The reinforcement corrosion reduces the section of the bars and the bearing capacity of a R.C. structural element. In the following we refer to a set of slender prismatic beams tested by Almusallam *et al.* (Almusallam *et al.* 1996, Almusallam 2001) and designed to collapse in bending under uniformly distributed load. Table 3 summarizes the dimensions of the beams. Table 4 lists the characteristics of the materials.

The specimens were subjected to a particular damaging process. Before the mechanical tests, the beams were immersed in a 5% NaCl solution and the bars were maintained at a different electrical potential. Then, when the chloride percentage in the concrete mass of a beam reached a certain value, the beam was loaded by an increasing distributed load until the collapse.

In the numerical modelling, the specimen was exposed to a uniform external chloride concentration equal to 5%. Due to the self-weight, the simply supported beams are bent and

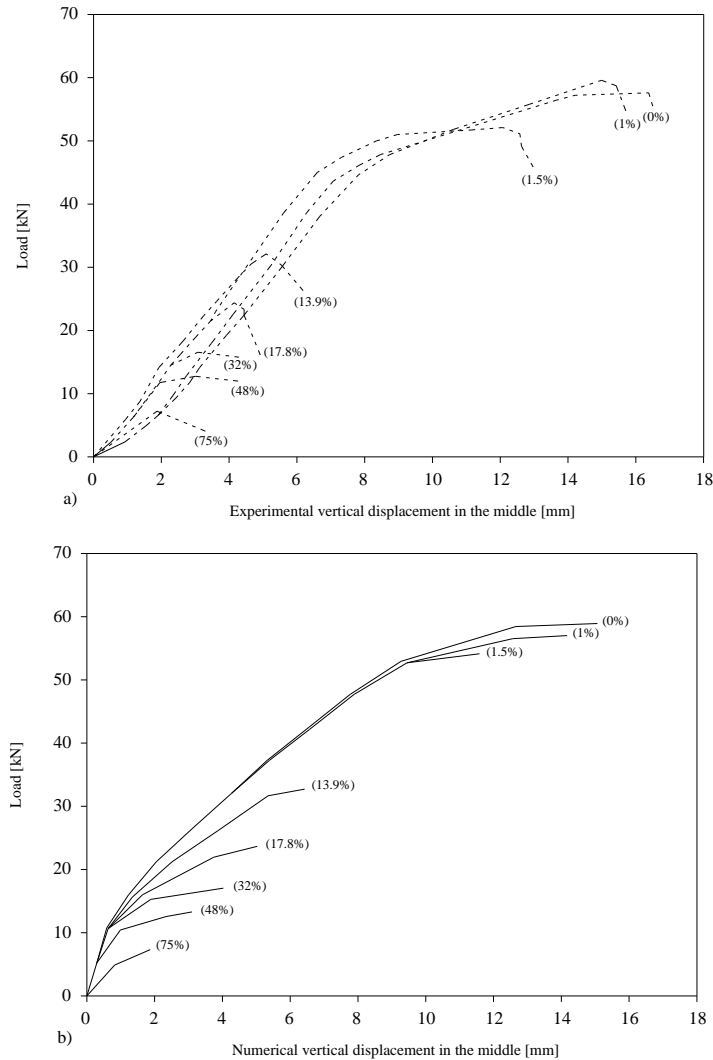


Fig. 10 Comparison between the numerical analysis and the experimental results obtained by Almusallam (1996). Load-displacement curves at different percentages of reinforcement corrosion: (a) Experimental tests; (b) numerical analysis

slightly cracked in the middle.

The numerical simulation of the chloride diffusion and of the corrosion process started from this initial condition. When the corrosion degrees reached one of the different levels considered in the experiments, the load was progressively increased until collapse.

Fig. 10(a) shows the experimental load-displacement curves at different percentages of reinforcement corrosion. Fig. 10(b) shows the corresponding curves obtained through the numerical analyses.

The model agrees with the experiments in representing how the progressive corrosion of the bars causes a corresponding reduction of the overall ductility and of the bearing capacity of the beams. In addition, the corresponding maximum load levels appear well approximated as well.

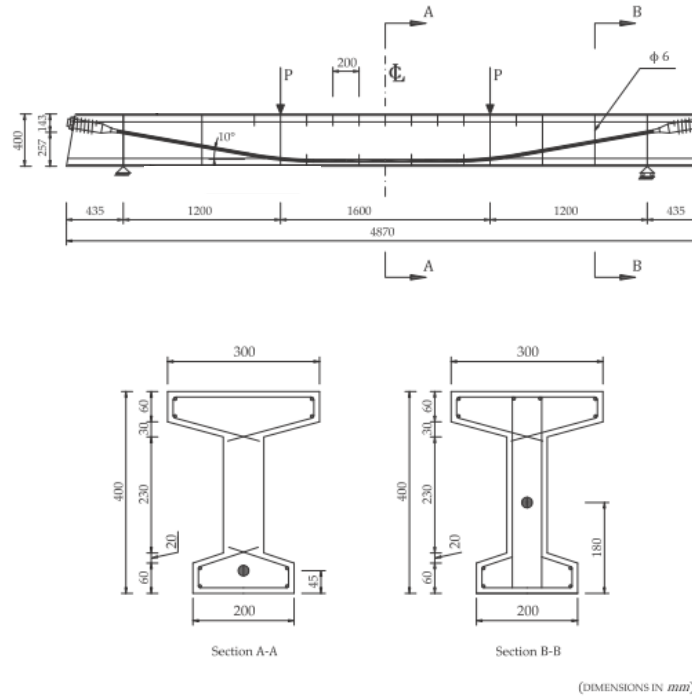


Fig. 11 “La Sapienza” RI 5 beam. Geometry, reinforcement layout and tendon profile

Table 5 Mechanical properties of materials (the values in brackets are not explicitly reported in the references, but assumed for computations)

Concrete	f'_c (MPa)	f_{cr} (MPa)	ε'_c (%)	E_s (MPa)
	-54.7	6.88	(-0.0025)	40400
Reinforcing steel	f_y (MPa)	f_u (MPa)	ε_{su} (%)	E_s (MPa)
	294	(460)	(20)	(196000)
Prestressed tendon	f_y (MPa)	f_u (MPa)	ε_{su} (%)	E_s (MPa)
	1610	(1800)	(5)	(196000)

At high corrosion levels, a relevant mechanical effect was detected both in the experimental and numerical analyses: failure modes, in fact, changed from flexural to shear type. Such a switch has some relevance for R.C. beams, in particular for those with small shear reinforcement, but it is critical for the prestressed concrete beams, in which the corrosion reduces both the sectional area of the strands and the compression action due to prestressing.

6. Analysis of prestressed concrete beams damaged by corrosion

Prestressed concrete beams subjected to uniform carbonation and localized chloride attack are now studied. The analyses are aimed at exploring the influence of these damaging agents and of their localization on the overall mechanical behaviour.

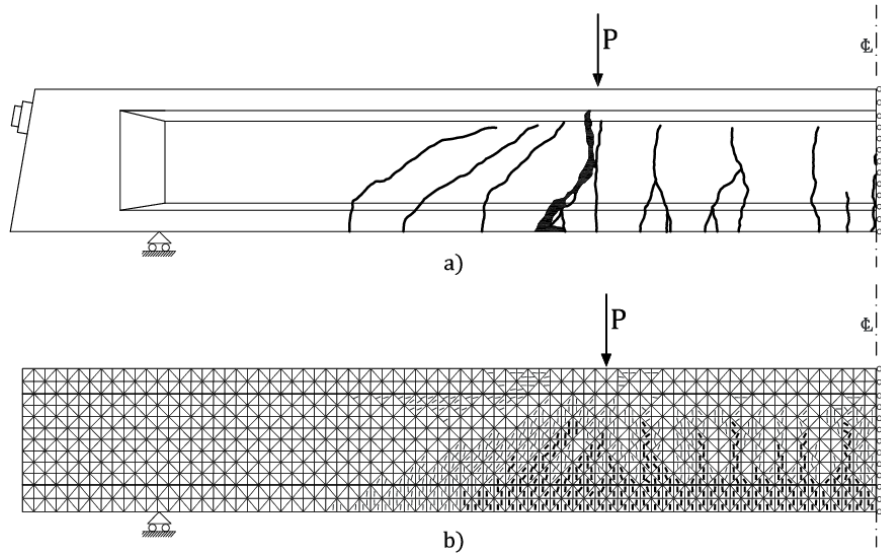


Fig. 12 Beam RI 5. Comparison between experimental (a) and numerical (b) crack patterns and between failure modes at the ultimate load $P_u=82$ kN (undamaged beam)

We refer to a prestressed concrete beam, called RI 5, belonging to a set of prestressed beams tested by Radogna (1965) at “La Sapienza”, Università di Roma (Rome) in 1960s. The geometry of the beam, the reinforcement layout and the tendon profile are shown in Fig. 11. The characteristics of the materials shown in Table 5 have been used.

6.1 Undamaged beam

Initially, the beam was studied without damage alterations in order to check the reliability of the mechanical solver only. Under an increasing loading, a systematic comparison among the numerical and experimental results was carried out. Comparisons regarded displacements, the onset and the propagation of cracking, the load deflection curve and the ultimate load. Fig. 12 shows a comparison between the experimental and numerical crack patterns and collapse mechanism at the ultimate load ($P_u=82$ kN)

6.2 Corrosion scenarios

We refer to the typical microclimate conditions surrounding a bridge girder and to the data recorded during years of survey activity on existing bridges. The external surfaces of the structural elements are considered as uniformly exposed to the carbon dioxide present in the atmosphere and hence the carbonation process is considered always active.

As noticed during the surveying activities, the worse damages on a bridge beam frequently happen in proximity of certain particular sections, where joints, niches or ducts belonging to the drainage system allow infiltration and stagnation of water or liquids containing deicing salts. So, the chloride attack is assumed as localised in narrow bands, where the chloride concentration is assumed to be distributed according to a bell distribution, having vertical axis at the middle of the band and given by Eq. (18)

Table 6 Damaging scenarios

Damaging scenario	Carbonation	Chloride attack
DS1	Uniform at both sides	At both sides near the bearing support
DS2	Uniform at both sides	At both sides in the middle of the shear zone
DS3	Uniform at both sides	At both sides at midspan

Table 7 Diffusion and corrosion parameters

K [mm/\sqrt{year}]	D_c [$mm^2/year$]	D_{cr} [$mm^2/year$]	i_{corr} [$mm/year$] (carbonation)	i_{corr} [$mm/year$] (chloride)
8	$1.6 \cdot 10^{14}$	$3.2 \cdot 10^{11}$	0.05	0.122

$$f(x) = \frac{1}{\sqrt{2 \cdot \pi \cdot \sigma^2}} \cdot \exp \left[-\frac{(x - \mu)^2}{2 \cdot \sigma^2} \right] \quad (18)$$

where μ and σ^2 are the average value (0) and the variance (0.16) of the bell distribution. The three different scenarios reported in Table 6 are investigated:

The concentration of chlorides on the surface was set at 2%, while the critical concentration for reinforcement is stated to be 0.5% of the cement weight. Diffusion and corrosion parameters are summarised in Table 7.

A concentrated load, equal to $0.60 P_{ult}$ is assumed.

6.2.1 Corrosion scenario CS1 (uniform carbonation and chloride attack near the bearing support)

The carbonation is assumed as uniform, while the band attacked by chloride is about 200 mm wide and localised at a distance of 230 mm from the support. Fig. 13 shows the crack patterns and a macrodivision of the shearing strain γ_{xy} at the onset of the collapse.

Fig. 16(a) shows the decrease of the tendon section over time. Corrosion starts after 24 years. Since then, the section of the tendon gradually decreases until the 35th year, when it abruptly vanishes. Fig. 16(b) shows the corresponding increase of the displacement at midspan. This displacement starts to increase after five years, as a consequence of the initial crack propagation and of minor corrosion effects, and goes on growing slowly. The breaking of the tendon after 35 years does not affect sensibly the time-deflection curve, which continues until the 60th year. The breaking of the tendon does not even influence the evolution of the shear strains and the crack pattern remains quite similar to that of the undamaged beam. In conclusion, a localized attack triggering corrosion near the support does not change the failure mode of this beam with respect to that in the undamaged state.

6.2.2 Corrosion scenario CS2 (uniform carbonation and chloride attack at the middle of the shear zone)

The carbonation is assumed to be uniform, while the band attacked by chloride is about 200 mm wide and localized at a distance of 630 mm from the support. Fig. 14 shows the crack patterns and a macrodivision of the shearing strain γ_{xy} at the onset of the collapse.

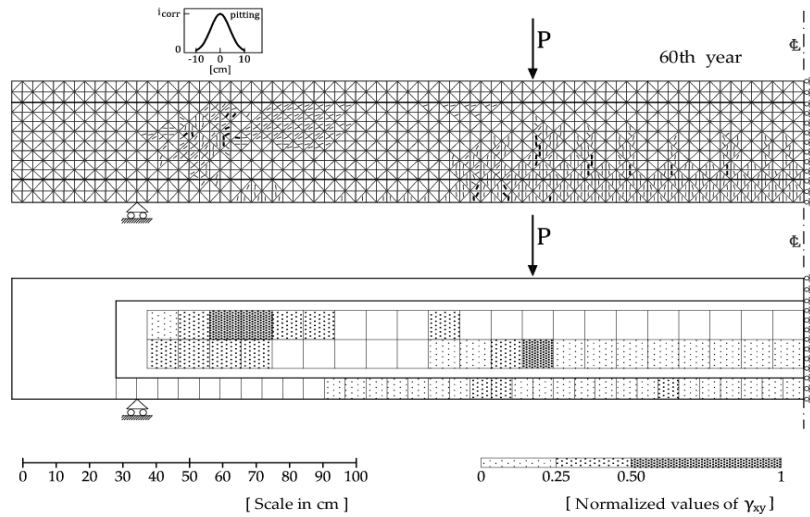


Fig. 13 Beam RI 5. Corrosion scenario CS1. Crack patterns and macrodivision of the shearing strain γ_{xy} , showing the failure mode at the onset of the collapse

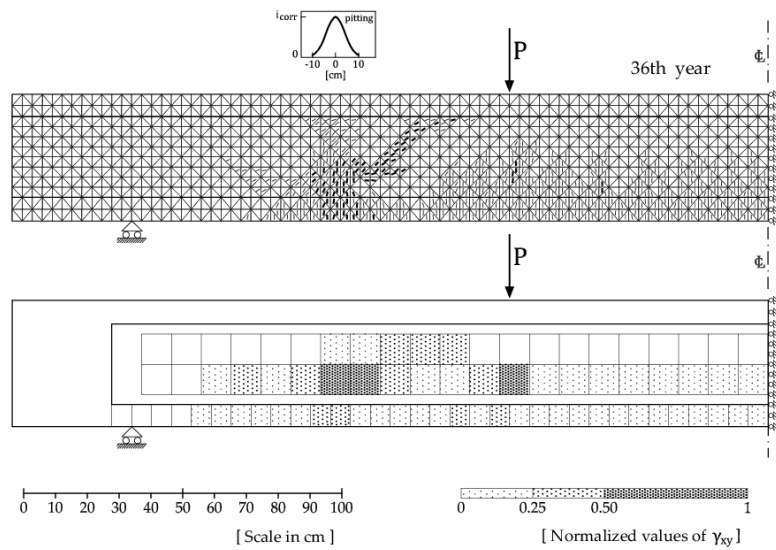


Fig. 14 Beam RI 5. Corrosion scenario CS2. Crack patterns and macrodivision of the shearing strain γ_{xy} , showing the failure mode at the onset of collapse

Fig. 16(a) shows how, as in the previous case, the corrosion starts after 24 years, while the tendon section decreases until the 36th year, when it reaches its breaking point (Fig. 16(a)). The displacement at midspan starts to increase after five years (Fig. 16(b)). However, in this case, when tendon breaks, the displacement diverges and the beam fails suddenly. The failure mode is not yet flexural, as in the undamaged beam. In the shear span, large shearing strains occur and the crack pattern shows newly-formed cracks, with a 45° orientation in the shear zone. Hence, a localized attack causing the corrosion of the tendon at the shear span changes the failure mode of the beam, which switches from flexural to shear type.

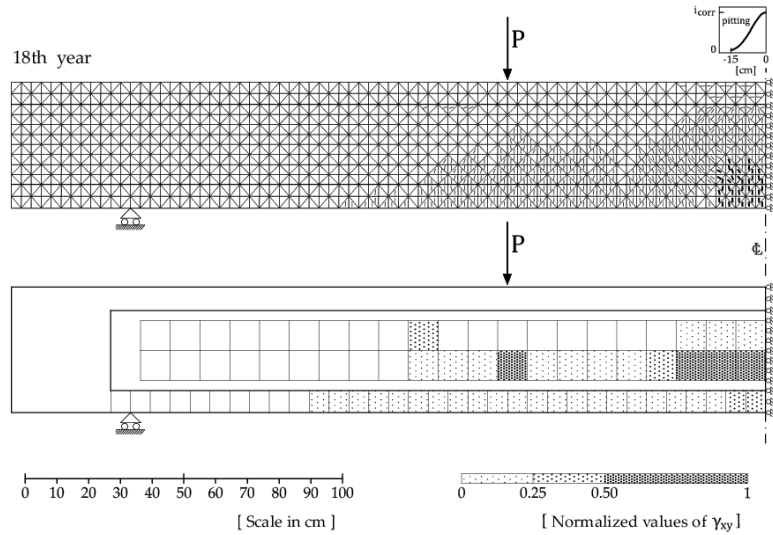


Fig. 15 Beam RI 5. Corrosion scenario CS3. Crack patterns and macrodivision of the shearing strain γ_{xy} , showing the failure mode, at the onset of collapse

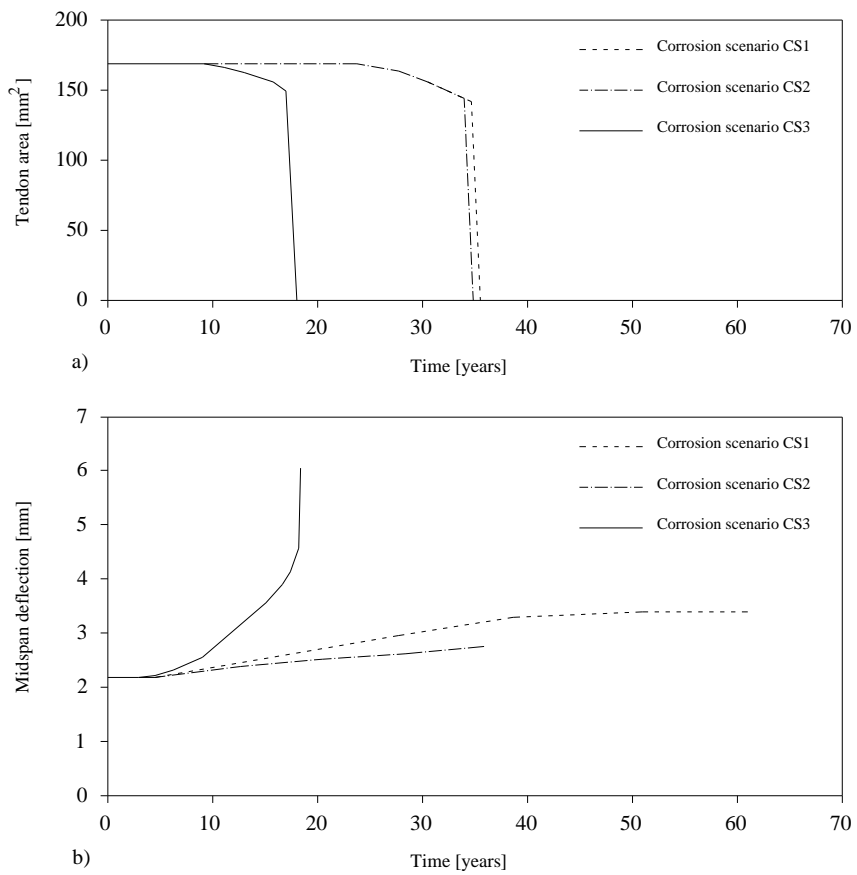


Fig. 16 RI 5 damaged beam. Comparison between prestressing deflections at midspan and tendon area for different corrosion scenarios CS1, CS2, CS3

6.2.3 Corrosion scenario CS3 (uniform carbonation and chloride attack at the midspan)

The carbonation is assumed to be uniform, while the band attacked by chloride is about 200 mm wide and localized across midspan. Fig. 15 shows the crack patterns and a macrodivision of the shearing strain γ_{xy} at the onset of the collapse.

As shown in Fig. 16(a), corrosion starts after nine years and the tendon section vanishes in at the 18th year. The displacement at midspan starts to increase after five years. After the 9th years, the displacement rapidly increases until the beam collapse, which occurs after 18 years. As one can see from Fig. 15, the failure mode remains flexural.

6.3 A comparison among the mechanical behavior in the three scenarios

As already shown, Fig. 16(a) summarizes the reduction over time of the sectional area of the prestressing tendon and Fig. 16(b) summarizes the increment over time of the mid-span displacement for the different scenarios CS1 CS3.

The onset of corrosion and the collapse caused by corrosion happen quite early when the attack occurs at midspan. Such a behavior can be attributed to the presence of more severe flexural cracks in the middle of the beam when a localized attack takes place. This accelerates the reinforcement degradation process with respect to the other scenarios, in which the attack occurs in areas not yet exhibiting cracks.

It is also important to compare the different collapse modes. Beam RI 5 was designed so that the collapse mechanism would be flexural. The macro division of the shearing strain zones, shown in Figs. 13-15, contributes in highlighting how the corrosion of the tendon may contribute in switching the failure mode from flexural to shear.

7. Conclusions

This paper presents a computational approach to the analysis of reinforced and prestressed concrete elements under long-term loading conditions, and subjected to given damaging scenarios. The effects of the diffusion of aggressive agents, of the onset and the development of the corrosion state in the reinforcement and the corresponding mechanical response are studied. As known, the corrosion on the reinforcing bars influences the damaging rate in the cracking pattern evolution; hence, the damage development and the mechanical behaviors are considered as coupled phenomena.

The model reliability is validated in studying the diffusion of the aggressive agents and the corresponding changes in the mechanical response of simple structural elements against experimental data is reported in Literature. These elements consist of simply supported reinforced concrete beams, subjected to carbonation and chloride. The benchmarks show how the analysis is able to reproduce the penetration rate of carbonation and chlorides at different levels of cracking, the progression of the steel corrosion process, the evolution of the cracking pattern and the influence of all those factors on the ultimate load carrying capacity.

A second set of applications concerns the behavior of a P.C. beam exposed to the attack of chlorides and carbonation. At first, the beam is studied in its sound state, for which the result of the experimental test are available. Then, the same beam is analyzed in damaged states, described by three different attack scenarios. The analyses highlight the influence of the degradation process on the non-linear response of the structure and on its failure mode. In particular, it is shown how,

depending on where the corrosive attack occurs, a beam designed for a flexural collapse in the sound state may switch to an earlier shear type collapse due to corrosion.

In synthesis, such modelling technique has proved to be able to catch the effects of the propagation of environmental aggressive agents, their evolution over the time and the time steps corresponding to the onset of critical service and/or ultimate states and the collapse mode.

Since many bridges that are more than 40-50 years old are clearly affected by damaged states, this approach may result in a useful contribution in assessing the structural reliability, the evolution of the residual bearing capacity and of the expediency, as well as the effectiveness of repairing actions. These are the reasons why it could play an important role in the infrastructure management.

References

- Almusallam, A.A. (2001), "Effect of degree of corrosion on the properties of reinforcing steel bars", *Constr. Build. Mater.*, **15**(8), 361-368.
- Almusallam, A.A., Al-Gahtani, A.S., Aziz, A.R., Dakhil, F.H. and Rasheeduzzafar, F. (1996), "Effect of reinforcement corrosion on flexural behavior of concrete slabs", *J. Mater. Civil Eng.*, **8**(3), 123-127.
- Bertolini, L., Elsener, B., Pedferri, P. and Polder, R.P. (2004), *Corrosion of Steel in Concrete: Prevention, Diagnosis, Repair*, WILEY-VCH Verlag GmbH & Co. KGaA, Weinheim, Germany.
- Biondini, F., Malerba, P.G. and Frangopol, D.M. (2006), "Time-variant performance of the certosa cable-stayed bridge", *Struct. Eng. Int.*, **16**(3), 235-244.
- Bontempi, F., Barbera, F. and Malerba, P.G. (1996), "Semianalytical finite strip analysis of reinforced concrete structures", *Proceedings of the 3rd Asian Pacific Conference on Computational Mechanics*, Seoul, South Korea, September.
- Boulfiza, M., Sakai, K., Banthia, N. and Yoshida, H. (2003), "Prediction of chloride ions ingress in uncracked and cracked concrete", *ACI Mater. J.*, **100**(1), 38-48.
- Breysse, D. (1997), *Transport of Fluids in Cracked Media, Penetration and Permeability of Concrete*, RILEM Report 16, Penetration and Permeability of Concrete, 123-153.
- Castel, A., François, R. and Arliguie, R. (1999), "Effect of loading on carbonation penetration in reinforced concrete elements", *Cement Concrete Res.*, **29**(4), 561-565.
- Castel, A., François, R. and Arliguie, R. (2000), "Mechanical behaviour of corroded reinforced concrete beams-part I: Experimental study of corroded beams", *Mater. Struct.*, **33**(9), 539-544.
- Coronelli, D., Castel, A., Anh, V.N. and François, R. (2009), "Corroded post-tensioned beams with bonded tendons and wire failure", *Eng. Struct.*, **31**(8), 1687-1697.
- Darmawan, M.S. and Stewart, M.G. (2007), "Effect of pitting corrosion on capacity of prestressing wires", *Mag. Concrete Res.*, **59**(2), 131-139.
- Ekolu, S.O. (2016), "A review on effects of curing, sheltering, and CO₂ concentration upon natural carbonation of concrete", *Constr. Build. Mater.*, **127**, 306-320.
- El Hassan, J., Bressolette, P., Chateauneuf, A. and El Tawil, K. (2010), "Reliability-based assessment of the effect of climatic conditions on the corrosion of RC structures subject to chloride ingress", *Eng. Struct.*, **32**(10), 3279-3287.
- Garavaglia, E., Sgambi, L. And Basso, N. (2012), "Selective maintenance strategies applied to a bridge deteriorating steel truss", *Proceedings of the 6th International Conference on Bridge Maintenance, Safety and Management*, Stresa, Italy, July.
- Goins, D. (2000), "Motor speedway bridge collapse caused by corrosion", *Mater. Perform.*, **36**(7), 18-19.
- Gonzalez, J.A., Andrade, C., Alonso, C. and Feliu, S. (1995), "Comparison of rates of general corrosion and maximum pitting penetration on concrete embedded steel reinforcement", *Cement Concrete Res.*, **25**(2), 257-264.

- Isecke, B. (1983), "Collapse of the Berlin congress hall prestressed concrete roof", *Mater. Perform.*, **21**(12), 36-39.
- Jacobsen, S., Sellevold, E. and Matala, S. (1996), "Frost durability of high strength concrete: Effect of internal cracking on ice formation", *Cement Concrete Res.*, **26**(6), 919-931.
- Köliö, A., Pakkala, T.A., Lahdensivu, J. and Kiviste M. (2014), "Durability demands related to carbonation induced corrosion for Finnish concrete buildings in changing climate", *Eng. Struct.*, **62-63**, 42-52.
- Lu, Z.H., Ou, Y.B., Zhao, Y.G. and Li, C.Q. (2016), "Investigation of corrosion of steel stirrups in reinforced concrete structures", *Constr. Build. Mater.*, **127**, 293-305.
- Malerba, P.G. (2014), "Inspecting and repairing old bridges: Experiences and lessons", *Struct. Infrastruct. Eng.*, **14**(4), 443-470.
- Malerba, P.G. and Sgambi, L. (2014), "Riveted steel elements deformed by the swelling of interstitial rust. A study on a residual bearing capacity", *Proceedings of the 7th International Conference on Bridge Maintenance, Safety and Management*, Shanghai, China, July.
- Malumbela, G., Alexander, M. and Moyo, P. (2009), "Steel corrosion on RC structures under sustained service loads-a critical review", *Eng. Struct.*, **31**(11), 2518-2525.
- Michel, A., Otieno, M., Stang, H. and Geiker, M.R. (2016), "Propagation of steel corrosion in concrete: Experimental and numerical investigations", *Cement Concrete Compos.*, **70**, 171-182.
- Nürnbergger, U. (2002), "Corrosion induced failure mechanisms of prestressing steel", *Mater. Corros.*, **53**(8), 591-601.
- Otsuki, N., Miyazato, S., Diola, N.B. and Suzuki, H. (2000), "Influences of bending crack and water-cement ratio on chloride-induced corrosion of main reinforcing bars and stirrups", **97**(4), 454-464.
- Palermo, A., Gil-Martin, L.M., Hernandez-Montes, E. and Aschheim, M. (2014), "Refined compression field theory for plastered straw bale walls", *Constr. Build. Mater.*, **58**, 101-110.
- Paulík, P., Bacuvčík, M., Ševčík, P. and Janotka, I. (2016), "Material properties and carbonation depths measured on seven, more than a 100-years old concrete bridges in Slovakia", *Proc. Eng.*, **156**, 326-333.
- Radogna, E.F. (1965), *Nota Informativa su Esperienze in Corso sul Comportamento a Taglio di Travi Precomprese a Cavi Post-Tesi, Atti delle Giornate del Precompresso*, Ravello, 24-30.
- Sarja, A. and Vesikari, E. (1996), *Durability Design of Concrete Structures*, RILEM Report Series 14, RILEM Technical Committee 130-CSL, E & FN Spon, London, U.K.
- Schiessl, P. and Lay, S. (2005), *Influence of Concrete Composition, Corrosion in Reinforced Concrete Structures*, Woodhead Publishing, Cambridge, 91-134.
- Sgambi, L. (2004), "Fuzzy theory based approach for three-dimensional nonlinear analysis of reinforced concrete two-blade bridge piers", *Comput. Struct.*, **82**(13-14), 1067-1076.
- Sgambi, L. (2014), "Influence of degradation at the base of a support post in a collapse of an old guardrail: A forensic analysis", *Eng. Fail. Anal.*, **42**, 284-296.
- Sgambi, L., Bontempi, F. and Garavaglia, E. (2006), "Structural response evaluation of two-blade bridge piers subjected to a localized deterioration", *Proceedings of the 3rd International Conference on Bridge Maintenance, Safety and Management*, Porto, Portugal, July.
- Sgambi, L., Gkoumas, K. and Bontempi, F. (2014), "Genetic algorithm optimization of precast hollow core slabs", *Comput. Concrete*, **13**(3), 389-409.
- Tuutti, K. (1982), *Corrosion of Steel in Concrete*, CBI Research Report No. 4.82, Swedish Foundation for Concrete Research, Stockholm, Sweden.
- Val, D.V., Stewart, M.G. and Melchers, R.E. (1998), "Effect of reinforce corrosion on reliability of highway bridges", *Eng. Struct.*, **20**(11), 1010-1019.
- Vecchio, F.J. (1989), "Non-linear finite element analysis of reinforced concrete membranes", *ACI Struct. J.*, **86**(1), 26-35.
- Vecchio, F.J. and Collins, M.P.C. (1986), "The modified compression-field theory for reinforced concrete elements subjected to shear", *ACI Struct. J.*, **83**(2), 219-231.
- Vesikari, E. (1988), "Service life prediction of concrete structures with regard to corrosion of reinforcement", Research Report NA 553, Technical Research Center of Finland (VTT), Finland.
- Vidal, T., Castel, A. and François, R. (2007), "Corrosion process and structural performance of a 17 year old

- reinforced concrete beam stored in chloride environment”, *Cement Concrete Res.*, **37**(11), 1551-1561.
- Vořechovská, D., Podroužek, J., Chromá, M., Rovnaníková, P. and Teplý, B. (2009), “Modeling of chloride concentration effect on reinforcement corrosion”, *Comput.-Aid. Civil Infrastr. Eng.*, **24**(6), 446-458.
- Woodward, R.J. and Williams, F.W. (1988), “Collapse of ynys-y-gwas bridge, west glamorgan”, *Proceedings of the Institution of Civil Engineers*, Part I 84, 634-669.
- Zhang, Y.F., Torgal, F. and Zhang, Y. (2012), “Shear behaviour of steel fibre reinforced self-consolidating concrete beams based on the modified compression field theory”, *Compos. Struct.*, **94**(8), 2440-2449.

CC

Appendix: Sectional area reduction due to pitting

Referring to Fig. 2, the following geometrical relationships between pit depth and reduced cross-sectional area of a rebar come out.

$$a(t) = 2 \cdot p(t) \cdot \sqrt{1 - \left[\frac{p(t)}{D_0} \right]^2} \quad (a)$$

$$\theta_1(t) = 2 \cdot \arcsin \left[\frac{a(t)}{D_0} \right] \quad (b)$$

$$\theta_2(t) = 2 \cdot \arcsin \left[\frac{a(t)}{2 \cdot p(t)} \right] \quad (c)$$

$$A_1(t) = 0.5 \cdot \left[\theta_1(t) \cdot \left(\frac{D_0}{2} \right)^2 - a(t) \cdot \left| \frac{D_0}{2} - \frac{p(t)^2}{D_0} \right| \right] \quad (d)$$

$$A_2(t) = 0.5 \cdot \left[\theta_2(t) \cdot p(t)^2 - a(t) \cdot \frac{p(t)^2}{D_0} \right] \quad (e)$$

$$A_{\text{pit}}(t) = \begin{cases} A_1 + A_2 & \text{se } p(t) \leq \frac{D_0}{2} \\ \frac{\pi \cdot D_0^2}{4} - A_1 + A_2 & \text{se } \frac{D_0}{2} < p(t) \leq D_0 \\ \frac{\pi \cdot D_0^2}{4} & \text{se } p(t) > D_0 \end{cases} \quad (f)$$

$$A_s(t) = \frac{\pi \cdot D_0^2}{4} - A_{\text{pit}}(t) \quad (g)$$